

Photoinduced Charge Separation in a Ferrocene–Aluminum(III) Porphyrin–Fullerene Supramolecular Triad[†]

Prashanth K. Poddutoori,[‡] Atula S. D. Sandanayaka,[§] Taku Hasobe,^{*,§,||} Osamu Ito,^{*,⊥} and Art van der Est^{*,‡}

Department of Chemistry, Brock University, 500 Glenridge Avenue, St. Catharines, ON, Canada, L2S 3A1, School of Materials Science, Japan Advanced Institute of Science and Technology, Asahidai, Nomi, 923-1292, Japan, PRESTO, Japan Science and Technology Agency (JST), 4-1-8 Honcho, Kawaguchi, Saitama, 332-0012, Japan, and IMRAM, Tohoku University, Katahira, Sendai, 980-8577 Japan

Received: December 17, 2009; Revised Manuscript Received: February 26, 2010

Light-induced electron transfer is investigated in a ferrocene–aluminum(III) porphyrin–fullerene supramolecular triad (FcAlPorC_{60}) and the constituent dyads (AlPorC_{60} and FcAlPorPh). The fullerene unit (C_{60}) is bound axially to the aluminum(III) porphyrin (AlPor) via a benzoate spacer, and ferrocene (Fc) is attached via an amide linkage to one of the four phenyl groups in the meso positions of the porphyrin ring. The absorption spectra and voltammetry data of the complexes suggest that the ground state electronic structures of the Fc , AlPor , and C_{60} entities are not significantly perturbed in the dyads and triad. Time-resolved optical and transient electron paramagnetic resonance (EPR) data show that photoexcitation of the AlPorC_{60} dyad results in efficient electron transfer from the excited singlet state of the porphyrin to fullerene, producing the charge-separated state $\text{AlPor}^{+}\text{--C}_{60}^{-}$. The fluorescence and transient EPR data also suggest that some energy transfer from the porphyrin to fullerene may occur. The lifetime of the radical pair $\text{AlPor}^{+}\text{--C}_{60}^{-}$ measured by transient absorbance spectroscopy is found to be 39 ns in *o*-dichlorobenzene at room temperature. At 200 K, transient EPR experiments place a lower limit of 5 μs on the radical pair lifetime. In the triad, the data suggest that excitation of the porphyrin gives rise to the charge-separated state $\text{Fc}^{+}\text{--AlPor--C}_{60}^{-}$ in two electron transfer steps. Photocurrent measurements demonstrate that both dyads and the triad have good photovoltaic performance. However, when Fc is appended to AlPorC_{60} , the expected improvement of the radical pair lifetime and the photovoltaic characteristics is not observed.

Introduction

The development of artificial photosynthetic complexes that mimic the energy and electron transfer processes of natural photosynthesis is a research area of growing importance.^{1–4} Metalloporphyrins (MPor) have been widely used in the design of such complexes^{5–8} because of their characteristic electrical, optical, and catalytic properties as well as their chemical, thermal, and light stabilities.⁹ Moreover, these properties can be modulated by varying the central metal or the substituents on the porphyrin. By attaching electron acceptors and donors either axially or equatorially to the porphyrin, artificial photosynthetic model systems^{10–13} and photovoltaic devices^{14–19} can be constructed. In such systems, fullerene (C_{60}) is attractive as an electron acceptor because it has a small reorganization energy, which tends to increase the rate of charge separation (CS) and decrease the rate of charge recombination (CR).^{3,20–25} Thus, the combination of MPor or metallophthalocyanines (MPc) and C_{60} building blocks has found widespread use for the construction of donor–acceptor complexes with the fullerene connected either covalently^{26–34} or noncovalently^{35–46} to the MPor or MPc. Since the first synthesis of a MPc– C_{60} dyad in 1995,²⁷ most of these models have the fullerene bound via a

bridging group to the periphery of the porphyrin ring. Thus, the major direction of electron transfer is horizontal as defined by the plane of the porphyrin. However, in natural photosynthesis, the electron transfer is mediated by axially bound amino acids and the direction of electron transfer in purple bacterial reaction centers has a significant out-of-plane component.⁴⁷ Because the nature of the orbital overlap between the donor and the acceptor is a crucial factor in the efficiency of electron transfer, there is an interest in mimicking the binding and arrangement of the natural system more closely. In addition, such an arrangement inhibits aggregation between porphyrin molecules, which is a widespread problem with synthetic model compounds. Thus, there have been a number of recent reports of compounds in which fullerene is attached such that electron transfer occurs in the vertical direction relative to the porphyrin plane. Examples include $\text{C}_{60}\text{--MPc--C}_{60}$ and $\text{C}_{60}\text{--MPor--C}_{60}$ triads,^{33,48} face-to-face pacman-type⁴⁹ and parachute topology⁵⁰ zinc(II) porphyrin–fullerene dyads, as well as self-assembled systems in which fullerene with an appended pyridyl or imidazole group is attached to zinc(II) porphyrin in the axial position via a coordination bond.^{37,40–43} Most of these systems show efficient electron transfer from the porphyrin to fullerene; however, stepwise or cascade electron transfer in the vertical direction has not been studied. One reason for this is the difficulty associated with attaching two different ligands to the porphyrin in the axial position.

Here, we explore the possibility of using Al(III) porphyrin to build a triad which undergoes multistep electron transfer in a direction primarily perpendicular to the porphyrin ring.

[†] Part of the “Michael R. Wasielewski Festschrift”.

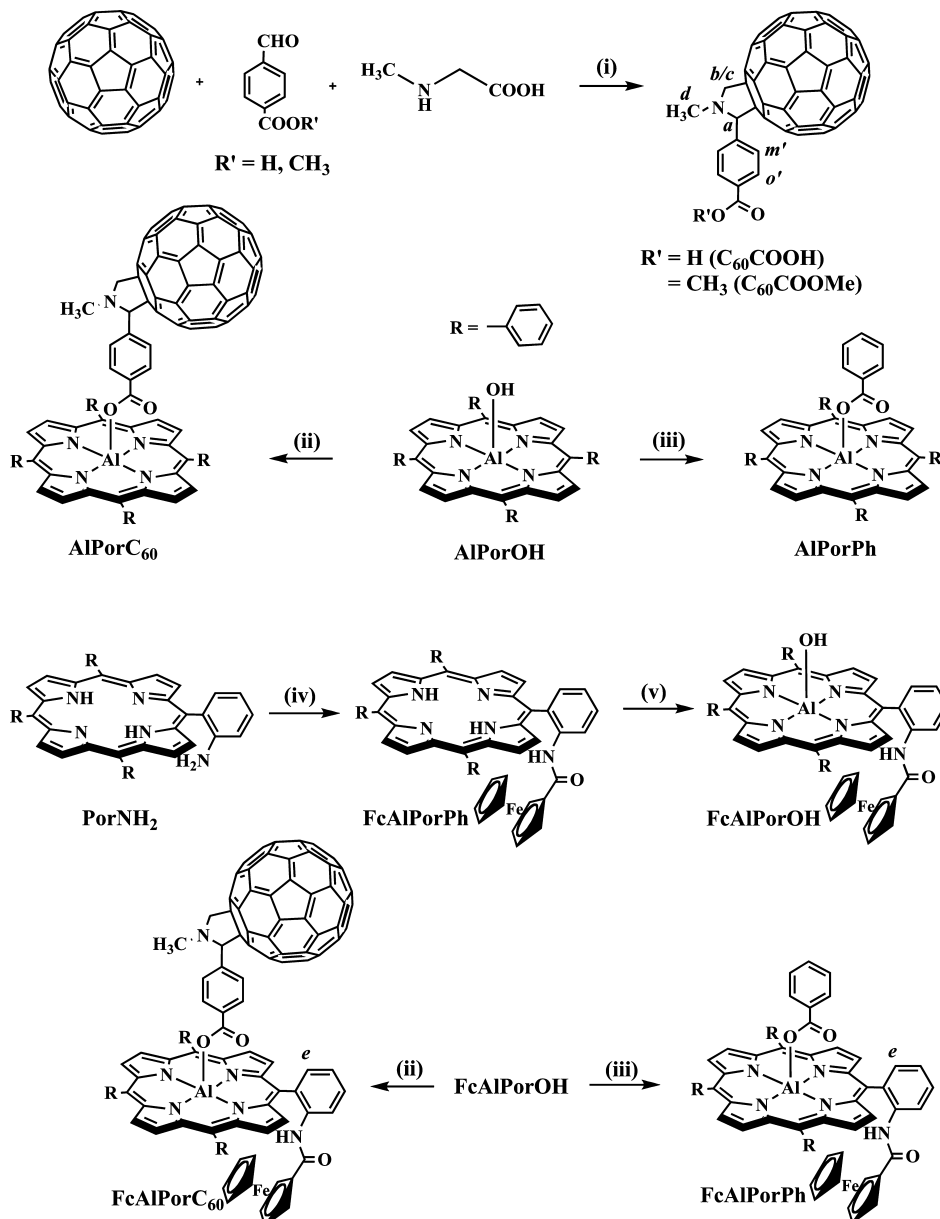
^{*} Corresponding authors. E-mail: t-hasobe@jaist.ac.jp (T.H.); ito@tagen.tohoku.ac.jp (O.I.); avde@brocku.ca (A.v.d.E.).

[‡] Brock University.

[§] Japan Advanced Institute of Science and Technology.

^{||} Japan Science and Technology Agency (JST).

[⊥] Tohoku University.

SCHEME 1: Synthetic Pathway to Al(III) Porphyrin Based Dyads and Triad^a

^a The following reagents and conditions were used: (i) toluene, reflux, 1–2 h; (ii) *N*-methyl-2-(*p*-benzoic acid)-3,4-fulleropyrrolidine (C₆₀COOH), toluene, reflux, 12 h; (iii) benzoic acid, dichloromethane (DCM); (iv) ferrocenecarbonyl chloride, pyridine, DCM, 4 h; (v) trimethylaluminum, toluene, 6 h; water, 12 h.

Aluminum(III) porphyrins have a number of distinctive properties which make them attractive for constructing such complexes: (i) they form axial covalent bonds with alcohols, carboxylic acids, and phosphinates,^{51–54} (ii) they have moderate redox potentials,⁵⁵ and (iii) they have a sixth coordination site^{56,57} available for binding external ligands. In this study, we take advantage of the first two of these features of Al(III) porphyrin to construct several functionally active donor–acceptor complexes, as shown in Scheme 1. We report two new Al(III) porphyrin based dyads (ferrocene–Al(III) porphyrin (FcAlPorPh) and Al(III) porphyrin–fullerene (AlPorC₆₀)) and a triad (ferrocene–Al(III) porphyrin–fullerene (FcAlPorC₆₀)) and study their photophysical properties by steady-state and time-resolved spectroscopic techniques. These spectroscopic and electrochemical measurements show that the compounds undergo light-induced electron transfer and have high photovoltaic performances.

Experimental Section

Materials. Al(III) porphyrin based dyads (ferrocene–Al(III) porphyrin (FcAlPorPh) and Al(III) porphyrin–fullerene (AlPorC₆₀)) and a triad (ferrocene–Al(III) porphyrin–fullerene (FcAlPorC₆₀)) were synthesized according to Scheme 1. Details are described in the Supporting Information.

Methods. Steady-State Absorbance and Fluorescence. The UV–vis spectra were recorded with a ThermoSpectronic/Unicam UV-4 UV–vis spectrometer. Steady-state fluorescence spectra were recorded using a Photon Technologies International (London, Ontario) Quanta Master Model QM-2001 L-format, equipped with double-grating monochromators, a 150 W xenon lamp, and running Felix 32 software. For the fluorescence measurements, the concentrations of the compounds were adjusted so that they all had the same absorbance at an excitation wavelength of 550 nm.

Time-Resolved Fluorescence. The time-resolved fluorescence spectra were measured by a single photon counting method using a streakscope (Hamamatsu Photonics, C5680) as a detector and a laser (Hamamatsu Photonics M10306, laser diode head, 408 nm) as an excitation source. Lifetimes were evaluated with software included in the apparatus.

Transient Absorbance Measurements. Nanosecond transient absorption measurements were carried out using the second harmonic (532 nm) of a Nd:YAG laser (Spectra-Physics, Quanta-Ray GCR-130, 5 ns fwhm) as an excitation source. For transient absorption spectra in the near-IR region (600–1200 nm) and the time-profiles, monitoring light from a pulsed Xe lamp was detected with a Ge-APD (Hamamatsu Photonics, B2834). For the measurements in the visible region (400–1000 nm), a Si-PIN photodiode (Hamamatsu Photonics, S1722-02) was used as a detector.

Transient EPR. Transient EPR time/field data sets were recorded in direct-detection mode using a modified Bruker EPR 200D-SRC X-band spectrometer (Bruker Canada, Milton ON, Canada). This instrument response time is determined by the resonator bandwidth and is estimated to be ~50 ns. Optical excitation at 532 nm was achieved using 10 ns pulses from a Nd:YAG laser at a repetition rate of 10 Hz. EPR samples were prepared by dissolving the porphyrin complex under study in the *o*-dichlorobenzene (*o*-DCB) to a concentration of ~ 10^{-4} M. The solutions were placed in suprasil EPR sample tubes (4 mm o.d.) and were degassed by several freeze–pump–thaw cycles and then sealed under a vacuum.

Voltammetry. Cyclic and differential pulse voltammetric experiments (*o*-DCB, 0.1 M tetrabutylammoniumperchlorate (TBAP)) were performed on a BAS Epsilon electrochemical analyzer (working electrode, glassy carbon; auxiliary electrode, Pt wire; reference electrode, Ag). A Fc^+/Fc (Fc = ferrocene) couple was used to calibrate the redox potential values.

Photoelectrochemical Measurements. Suspensions of $(\text{C}_{60}\text{COOMe})_n$, $(\text{AlPorC}_{60})_n$, $(\text{FcAlPorPh})_n$, and $(\text{FcAlPorC}_{60})_n$ were prepared by injecting 0.5 mL of a 0.30 mM solution of each compound in *o*-DCB into 3 mL of acetonitrile solution at room temperature. The particle size in the suspension was then measured using dynamic light scattering and electron microscopy. The electrophoretic deposition method was used to deposit the dyads and triad onto an OTE/SnO₂ electrode, and photocurrent measurements were carried out as described in detail previously.^{58,59} Suspensions were transferred to a 1 cm cuvette in which two optically transparent electrodes were kept at a distance of 6 mm using a Teflon spacer. A DC electric field (~200 V/cm) was applied for 1 min between these two electrodes using a Power Pac HV (Bio-Rad). Photocurrent action spectra were recorded using a standard two-compartment cell consisting of a working electrode and a Pt wire gauze counter electrode in the electrolyte (0.5 M LiI and 0.01 M I₂ in acetonitrile). In the case of incident photon-to-electron conversion efficiency (IPCE) measurements, a monochromator (SM-25, Bunkoh-Keiki Co., Ltd.) was introduced into the path of the excitation beam (300 W xenon lamp, Bunkoh-Keiki Co., Ltd.) for the selected wavelength. The lamp intensity at each wavelength was determined using a Si photodiode (Hamamatsu Photonics S1337-1010BQ) and was corrected for.

Electron Micrograph Measurements. Transmission electron micrograph (TEM) measurements were performed by applying a drop of the sample to a copper grid. Images were recorded on a Hitachi H 7100 transmission electron microscope at an accelerating voltage of 100 kV for imaging.

Dynamic Light Scattering (DLS) Measurements. The particle size and distribution were measured in *o*-DCB/acetonitrile = 1/6, v/v, using light scattering equipment (Zetasizer nano ZS).

Results and Discussion

Syntheses. The synthetic route to the AlPor dyads and the triad is shown in Scheme 1 and described in detail in the Supporting Information. Briefly, the preparation of the dyad AlPorC₆₀ was achieved quantitatively using the condensation reaction between Al(III) porphyrin and carboxylic acid derivative of fullerene (step ii). Preparation of triad (FcAlPorC₆₀) involves three steps: First, ferrocene was attached to free-base porphyrin through an amide linkage (step iv). Then, Al(III) was inserted in the porphyrin cavity (step v). Lastly, C₆₀ was bound in the axial position of the porphyrin though a carboxylate linkage in a similar manner to step ii. The reference compounds AlPorPh and C₆₀COOMe were used for control experiments in all spectroscopic studies.

Structural characterization of these new compounds was carried out by NMR, mass spectroscopy, UV–vis absorption spectroscopy, and voltammetry, and the details are given in the Supporting Information. Successful attachment of the axial ligand to AlPorOH is confirmed by the FAB mass spectra which show an $[\text{M}]^+$ molecular ion peak and an $[\text{M} - \text{ACOO}]^+$ peak corresponding to loss of the axial ligand (A = phenyl or fullerene) from the Al(III) porphyrin. It is also supported by the upfield shift of the NMR signals from the *ortho* (*o'*) and *meta* (*m'*) protons of the benzoate linker and protons *a*–*d* of the pyrrolidine ring attached to the fullerene moiety (see Scheme 1). The upfield shift of the benzoate linker protons is due to the shielding effect of the porphyrin ring, and the measured shifts correlate with the anticipated distance of each proton from the porphyrin ring, confirming axial linkage *via* the carboxylate spacer. The triad FcAlPorC₆₀ and the reference compound FcAlPorPh can exist in two structural geometries with the Fc and C₆₀ (or Ph) substituents either on the same face or opposite faces of the porphyrin. Steric hindrance is expected to favor the conformation with substituents on opposite faces, as shown in Scheme 1. Interconversion of the two conformers should also be very restricted, because the amide linkage prevents rotation of the Fc substituent relative to the bridging phenyl group, which greatly increases the barrier to rotation of the phenyl group relative to the porphyrin ring. The chemical shift of proton *e* of the bridging phenyl group should be different for the two conformers, and indeed, two doublets are found at 8.84 and 8.89 ppm for this proton in the NMR spectrum of FcAlPorPh (Figure S6, Supporting Information). Together, the two peaks integrate as one proton with the doublet at 8.89 ppm accounting for 15–20% of the total intensity. Thus, we conclude that the two conformers are present in a 80:20 ratio with the sterically hindered conformer in which the Fc and Ph are on the same face being the minor component. In the case of the triad FcAlPorC₆₀, the ¹H NMR spectrum (Figure S7, Supporting Information) shows only one doublet for proton *e*, indicating that the presence of the bulky C₆₀ group prevents formation of the sterically hindered conformer in detectable amounts for this compound.

UV–Visible Absorption Spectroscopy. The absorption spectra of the new compounds (AlPorC₆₀, FcAlPorC₆₀, FcAlPorPh) and their reference analogues Fc, AlPorPh, and *N*-methyl-2-(*p*-methylbenzoate)-3,4-fulleropyrrolidine (C₆₀COOMe) measured in dichloromethane are shown in Figure 1, and the absorption maxima and extinction coefficients (λ_{max} and $\log \epsilon$) are summarized in Table S1 in the Supporting Information. The

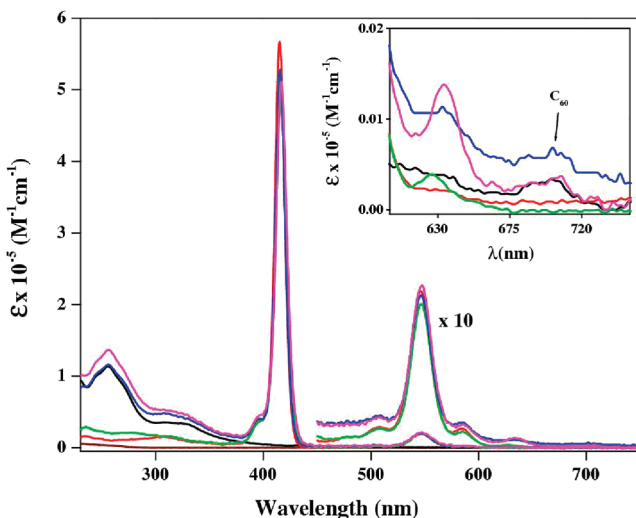


Figure 1. UV-visible absorption spectra of Fc (wine-red), $C_{60}COOMe$ (black), AlPorPh (red), AlPorC₆₀ (blue), FcAlPorPh (green), and FcAlPorC₆₀ (magenta) in CH_2Cl_2 . The inset shows a magnification of the 600–750 nm region with the weak band due to C_{60} indicated.

TABLE 1: Redox Potentials, Charge-Separated State Energies, and Free Energy Changes

sample	potential vs Fc/Fc ⁺ , V		E_{CS}^a , eV	ΔG_{CS}^a , eV	ΔG_{HS}^b , eV
	oxidation	reduction			
$C_{60}COOMe$		−1.17, −1.57, −2.12			
AlPorPh	0.38	−1.70, −2.07			
FcAlPorPh	0.14, 0.42	−1.63, −2.02	1.77 ^c	−0.37 ^d	
AlPorC ₆₀	0.35	−1.16, −1.54, −1.72, −2.09	1.51 ^e	−0.63 ^f	
FcAlPorC ₆₀	0.14, 0.40	−1.15, −1.55, −1.67, −2.06	1.55, ^e 1.29, ^g 1.81 ^c	−0.59, ^f −0.26 ^d	

^a $E_{CS} = e(E_{1/2}(D^{+*}/D) - E_{1/2}(A/A^{-}))$, where $E_{1/2}(D^{+*}/D)$ is the first oxidation potential of the donor and $E_{1/2}(A/A^{-})$ is the first reduction potential of the acceptor. ^b $\Delta G_{CS} = E_{CS} - E_{0-0}$. E_{0-0} is the energy of the lowest excited state of AlPor (2.14 eV). $\Delta G_{HS} = E_{CS}(AlPor-C_{60}) - E_{CS}(Fc-C_{60})$. $G_{CP} = -E_{CS}$. ^c $E_{CS}(Fc-AlPor)$. ^d $\Delta G_{HS}(Fc-AlPor)$. ^e $E_{CS}(AlPor-C_{60})$. ^f $\Delta G_{CS}(AlPor-C_{60})$. ^g $E_{CS}(Fc-C_{60})$.

absorption spectra of the dyads and triad are essentially a superposition of those of the individual chromophores. The porphyrin moiety shows the very strong B-band (Soret band) at ~416 nm and weak Q-band at ~547 nm typical of a metalloporphyrin. The fullerene-containing compounds have a strong $\pi-\pi^*$ transition band at ~256 nm and a very weak intensity band at ~700 nm, as shown in the inset. Ferrocene has an electronic transition at 442 nm, with low molar absorptivity, but it is hidden beneath the intense porphyrin and fullerene bands. From the absorption wavelengths and ϵ values obtained from the spectra, it is clear that there is no detectable perturbation of the ground-state electronic structures of the chromophores in the dyads and triad.

Voltammetry Measurements. Determination of the redox potentials of the compounds is important for evaluating the energetics of the electron transfer reactions and possible electronic interactions between the components of the complexes. Table 1 lists the redox midpoint potentials ($E_{1/2}$) of the dyads (FcAlPorPh, AlPorC₆₀), triad (FcAlPorC₆₀), and the reference compounds (AlPorPh, $C_{60}COOMe$) obtained from the voltammograms taken in 0.1 M TBAP *o*-DCB. Representative voltammograms are shown in Figure S8 in the Supporting Information. All of the redox processes of the compounds were found to be reversible or quasi-reversible based on the peak-

to-peak separation values and the cathodic-to-anodic peak current ratio.⁶⁰ Those of the dyads and triad are assigned to oxidation/reduction of the ferrocene, Al(III) porphyrin, and/or fullerene units by comparison to the appropriate reference compounds. For AlPorPh and FcAlPorPh, two reduction processes are observed and are assigned to the first and second reduction of the porphyrin. In contrast, for the dyad AlPorC₆₀, four reduction processes were observed. The first two are assigned to the reduction of fullerene and the third to the first reduction of the porphyrin. The fourth process is a combination of the third reduction of fullerene and the second reduction of the porphyrin. Similar reduction behavior is observed for the triad FcAlPorC₆₀.

In the anodic scan, the first oxidation of the porphyrin is easily identified for AlPorPh and AlPorC₆₀ but the second oxidation is difficult to discern; therefore, only the first oxidation potential is reported in Table 1. For FcAlPorPh and FcAlPorC₆₀, oxidation of the ferrocene unit is observed at lower potential. Similar to the absorption data, the voltammograms suggest that the components of the dyads and triad do not influence one another significantly. These redox potentials can be used to estimate the energy of the charge-separated state E_{CS} (relative to the ground state) and the free-energy changes for charge separation (ΔG_{CS}) and hole stabilization (ΔG_{HS}) using the Rehm and Weller method,^{61,62} as summarized in Table 1. For these calculations, we have ignored the stabilization energy due to the Coulomb interaction of the charges. The energy of the lowest excited state of the AlPor unit has been estimated from the position of the blue edge of the fluorescence spectrum at 579 nm. The calculated free energy changes suggest that electron transfer from the excited singlet state of AlPor (¹AlPor*) to fullerene and hole stabilization onto ferrocene are both energetically favorable. The energies obtained from the absorbance spectra and voltammetry data are also summarized in the energy-level diagrams of FcAlPorPh, AlPorC₆₀, and FcAlPorC₆₀ in *o*-DCB shown in Figure 2.

Fluorescence Studies. The steady-state fluorescence spectra of the dyads, triad, and the reference compounds measured with 550 nm excitation in *o*-DCB are illustrated in Figure 3, and the emission maxima are summarized in Table 2. At this wavelength, all of the absorption is due to the porphyrin in AlPorPh and FcAlPorPh, whereas in AlPorC₆₀ and FcAlPorC₆₀ 95% of the absorption is by the AlPor moiety and the remaining 5% is by C_{60} . As seen in Figure 3, all of the compounds exhibit two bands located around 600 and 650 nm due to AlPor emission and the C_{60} containing dyad AlPorC₆₀ also shows fullerene fluorescence bands at ~714 and 794 nm. In the dyads AlPorC₆₀ and FcAlPorPh, the fluorescence bands located around 600 and 650 nm are strongly quenched (~99%) compared to those of the reference compound AlPorPh. In the FcAlPorC₆₀ triad, additional AlPor fluorescence quenching compared to the dyads is observed. This fluorescence quenching suggests that the porphyrin excited state is depopulated by processes such as energy transfer and electron transfer between the components.

The very weak absorption of Fc (Figure 2, wine-red trace) occurs in the UV, while the fluorescence bands of AlPor (Figure 3) are in the red region of the visible spectrum. Hence, the spectral overlap required for Förster energy transfer from AlPor to Fc is essentially zero. On the other hand, the electrochemical data suggest that $Fc^{+}-AlPor^{-}$ lies energetically below the excited singlet state of AlPor ($\Delta G_{CS} = -0.37$ eV). Consequently, electron transfer is the more likely explanation for the strong quenching of AlPor fluorescence for FcAlPorPh.

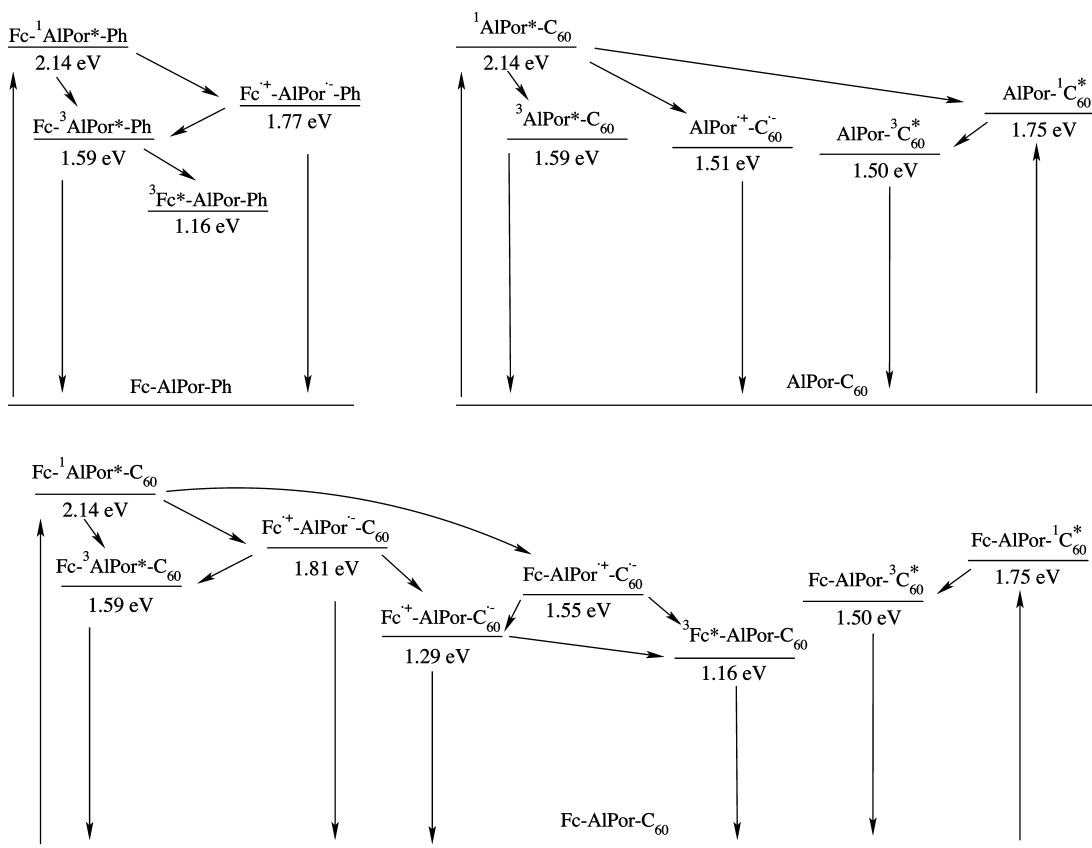


Figure 2. Energy level diagrams of FcAlPorPh, AlPorC₆₀, and FcAlPorC₆₀ in *o*-DCB.

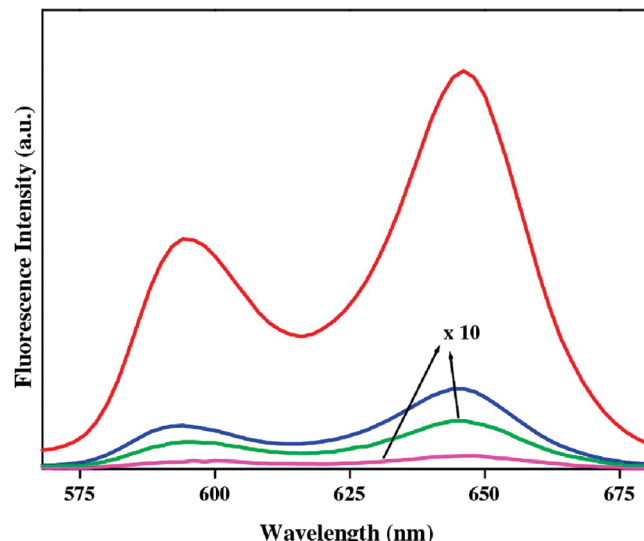


Figure 3. Steady-state fluorescence spectra of AlPorPh (red), AlPorC₆₀ (blue), FcAlPorPh (green), and FcAlPorC₆₀ (magenta) in *o*-DCB. All of the solutions had a concentration of 10 μM and were measured with an excitation wavelength of 550 nm. Note that the fluorescence intensity of FcAlPorPh and FcAlPorC₆₀ is multiplied by a factor of 10.

In the case of AlPorC₆₀, we also expect that electron transfer from ¹AlPor* to C₆₀ is the dominant quenching mechanism because the calculated value of ΔG_{CS} (−0.63 eV) is negative and the spectral overlap for energy transfer from ¹AlPor* to C₆₀ is also small (cf. Figure 2, black trace, Figure 3, red trace, and Figure S9 of the Supporting Information). However, energy transfer still may be feasible because of the absorbance of C₆₀ in the red region of the spectrum. On an expanded scale, the fluorescence spectrum of AlPorC₆₀ (Figure 4, blue trace) shows

a shoulder at ∼710 nm and a maximum at 790 nm. On the basis of a comparison with the emission spectra of AlPorPh (red trace) and C₆₀COOMe (black traces), we assign these features to the emission from C₆₀. (Note that the spectrum of AlPorPh (Figure 4, red trace) has been normalized to the intensity of the AlPorC₆₀ spectrum at 594 nm.) As is apparent in Figure 4, the intensity of the fullerene emission in the dyad is stronger than in C₆₀COOMe, suggesting that some energy transfer from ¹AlPor* to C₆₀ occurs.

In the case of the triad, FcAlPorC₆₀, additional fluorescence quenching is observed compared to AlPorPh and AlPorC₆₀ (Figure 3). However, unlike AlPorC₆₀, the triad FcAlPorC₆₀ does not exhibit increased C₆₀ fluorescence (data not shown). This suggests that emission from ¹AlPor* is quenched by electron transfer from Fc and that this process is faster than energy transfer C₆₀.

Fluorescence decay profiles of the dyads and triad measured using a time-correlated single-photon-counting apparatus with excitation at 408 nm are shown in Figure 5. The corresponding fluorescence lifetimes (τ_f(AlPor)) obtained by curve-fitting of the fluorescence decay in the 540–650 nm region with single and double exponential functions are summarized in Table 2. Consistent with the quenching of the steady-state fluorescence, the major decay components for AlPorC₆₀, FcAlPorPh, and FcAlPorC₆₀ are shorter than that of the reference sample AlPorPh. The singlet quenching rates, k_q^S, for ¹AlPor* were estimated from the difference between τ_f(AlPor) of the dyads and triad and τ_f(AlPor) of AlPorPh; these k_q^S values are listed in Table 2. Since energy transfer and other quenching processes are not expected in FcAlPorPh, k_q^S represents the hole-transfer rate to Fc (and possibly the enhanced rate of intersystem crossing) for this compound. For AlPorC₆₀, on the other hand, energy transfer and electron transfer to C₆₀ are possible and k_q^S

TABLE 2: Fluorescence Maxima, Lifetimes, and Quenching Rate Constants and Charge Recombination Rate Constants^a

sample ^b	λ_F/nm (Φ_F , %Q) ^c	$\lambda_{\text{em}}/\text{nm}$	τ_F/ns (%A) ^d	k_q^S/s^{-1} ($\Phi_q \times \%A$)	$k_{\text{CR}}/\text{s}^{-1}$ (τ_{RP})
C ₆₀ COOMe	712, 790	690–790	1.39 (100%)		
AlPorPh	594, 646 (0.153)	540–650	7.05 (100%)		
FcAlPorPh	603, 646 (0.004, 96)	540–650	0.10 (82%), 2.1 (18%)	1.00×10^{10} (0.98 × 0.82)	
AlPorC ₆₀	594, 644, 710, 790 (0.030, 80)	540–650 710–790	0.21 (90%), 2.90 (10%) 1.10 (30%), 0.06 (70%)	4.60×10^9 (0.97 × 0.90)	2.54×10^7 (39 ns)
FcAlPorC ₆₀	600, 648 (0.0005, 99)	540–650 710–790	0.07 (97%), 1.20 (3%) 0.80 (5%), 0.04 (95%)	1.46×10^{10} (0.99 × 0.97)	5.70×10^7 (17 ns)

^a Emission maxima (λ_F), fluorescence yield (Φ_F), percent quenching (%Q), emission range for time-resolved fluorescence (λ_{em}), fluorescence lifetimes (τ_F), relative amplitude of the decay component (%A), singlet state quenching rate constant (k_q^S), quantum yield of quenching process (Φ_q), charge recombination rate constant (k_{CR}), radical pair lifetime (τ_{RP}). ^b In *o*-DCB solution. ^c $\lambda_{\text{exc}} = 555$ nm. The fluorescence quantum yields (Φ_F) of these compounds were calculated by the steady-state comparative method using tetraphenylporphyrin (ZnTPP) as a reference ($\Phi_F = 0.036$ in CH₂Cl₂).^{63,64} Fluorescence quenching (%Q) = $[(\Phi_{\text{reference}} - \Phi_{\text{sample}})/\Phi_{\text{reference}}] \times 100$. ^d $\lambda_{\text{exc}} = 408$ nm. $k_q^S = (1/\tau)_{\text{sample}} - (1/\tau)_{\text{reference}}$, $\Phi_q = [(1/\tau)_{\text{sample}} - (1/\tau)_{\text{reference}}]/(1/\tau)_{\text{sample}}$.

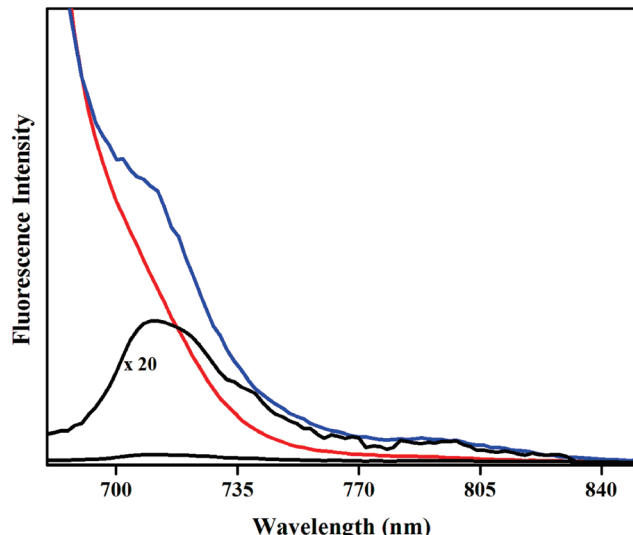


Figure 4. Fluorescence spectra of AlPorC₆₀ (blue), C₆₀COOMe (black), and AlPorPh (red) in *o*-DCB taken with an excitation wavelength of 550 nm. The spectrum of AlPorPh is normalized to the AlPorC₆₀ intensity at 594 nm.

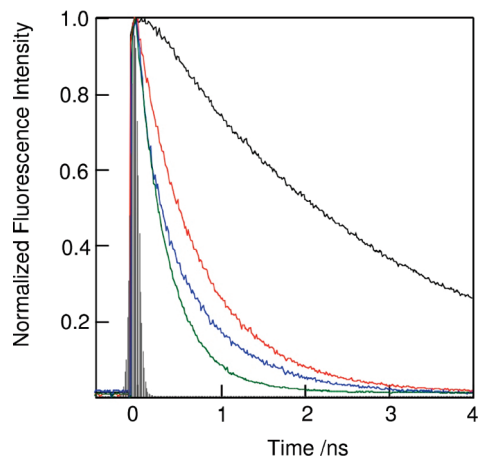


Figure 5. Fluorescence time profiles of AlPorPh (black), AlPorC₆₀ (red), FcAlPorPh (blue), and FcAlPorC₆₀ (green) in *o*-DCB monitored in the 540–650 nm region. $\lambda_{\text{ex}} = 408$ nm.

involves the rates of both processes. However, we expect electron transfer to be the dominant process because of the poor spectral overlap and low oscillator strength for C₆₀. For the triad FcAlPorC₆₀, the singlet-quenching rate is governed by electron transfer from Fc to ¹AlPor* in addition to energy and electron transfer to C₆₀. The rate constants given in Table 2 show that the singlet-quenching rates in the triad and in FcAlPorPh are a

factor of 2–3 greater than in AlPorC₆₀. Thus, it appears that the rate of electron transfer from ¹AlPor* to C₆₀ is about half that of electron transfer from Fc to ¹AlPor*.

Fluorescence time profiles of C₆₀COOMe, AlPorC₆₀, and FcAlPorC₆₀ taken in the 710–790 nm region to examine the emission from C₆₀ (Figure S10 in the Supporting Information) are biexponential. We assign the initial fast decay to AlPor fluorescence, whereas the slow minor component is due to C₆₀ emission. As shown in Table 2, the slow component in AlPorC₆₀ accounts for 30% of the total amplitude and its lifetime is estimated as 1.1 ns. This value is close to the 1.3 ns fluorescence lifetime of C₆₀COOMe, indicating that no significant quenching of ¹C₆₀* occurs in the dyad. By comparison, in FcAlPorC₆₀, the slow component accounts for only 5% of the total signal and has a lifetime of 0.8 ns. The lower amplitude is probably a result of a lower yield of energy transfer from ¹AlPor* to C₆₀ because ¹AlPor* is quenched by electron transfer from Fc. The reason for the somewhat shorter lifetime for the C₆₀ fluorescence is unclear.

Transient EPR Studies. Spin polarized transient EPR spectra of AlPorC₆₀ and C₆₀COOMe are shown in Figure 6. The spectra were taken in *o*-DCB at 200 K near the glass transition temperature of the solvent to increase the radical pair lifetime and slow the molecular motion that would otherwise make the transient EPR measurements unfeasible. In the top part of Figure 6, the spectrum of AlPorC₆₀ is compared to that of the triplet state of C₆₀ in C₆₀COOMe. The shape of the polarization patterns indicates that the triplet state is populated by spin-orbit coupling mediated intersystem crossing. A similar comparison with AlPorOH (not shown) indicates that the spin polarization of ³AlPor* is very weak in *o*-DCB even at 80 K; hence, the contribution of ³AlPor* is not observed in Figure 6.

In the case of AlPorC₆₀, a narrow feature is observed near 3465 G ($g \approx 2$). This region is shown on an expanded scale in the lower part of Figure 6 with a linear baseline correction applied to remove the sloping background from the C₆₀ triplet spectrum. The width of this feature and its polarization are similar to those reported for the radical pairs in other porphyrin–C₆₀ dyads,^{65–68} thus, we assign it to the radical pair AlPor*⁺C₆₀[−]. At lower temperature, the radical pair spectrum is not observed, because solvent reorganization is required to stabilize charge separation. At higher temperature, it is also not observed either because the polarization is averaged to zero or the radical pair lifetime is too short.

The radical pair spectrum in Figure 6 shows an A/E/A polarization pattern, which is not compatible with an immobilized radical pair triplet state. Thus, it may be subject to partial motional averaging because the spectrum has been measured above the melting point of the solvent. Under these

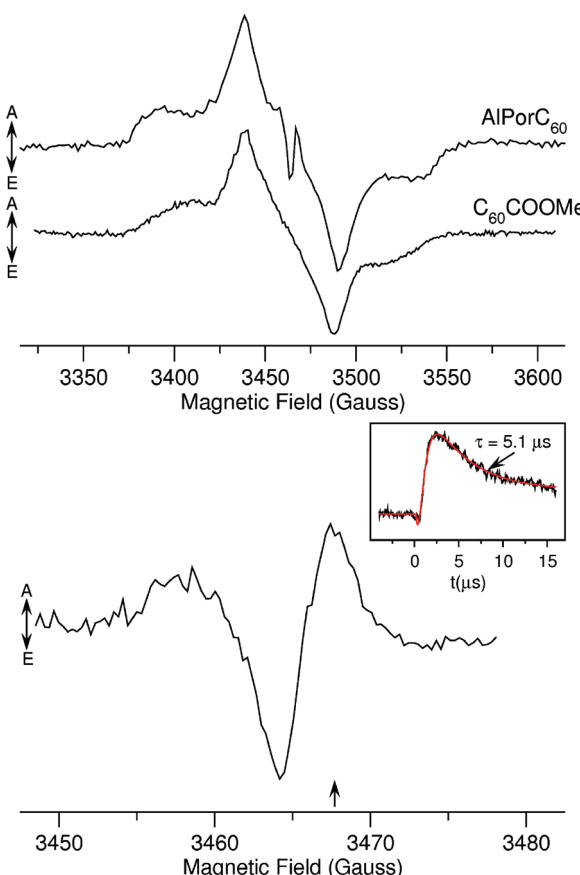


Figure 6. Spin polarized transient EPR spectra of AlPorC₆₀ and C₆₀COOMe in *o*-DCB at 200 K. Top: Wide scan showing the contribution from ³C₆₀. The spectra were extracted from the time/field data sets in a 200 ns wide window centered at 760 ns after the laser flash. Bottom: The spectra of AlPor⁺C₆₀[−] in the narrow region near $g \approx 2$ at 500 ± 100 ns with a linear baseline correction to remove the sloping background due to ³C₆₀. The inset shows the time trace at the magnetic field position indicated by an arrow under the spectrum.

conditions, even a qualitative analysis of the spectrum in terms of the strength of the dipolar coupling and the nature of the precursor state is difficult. At later times, spin relaxation causes the polarization pattern of the radical pair to evolve to a purely absorptive spectrum, which then decays with a lifetime of 5 μs , as shown in the inset in Figure 6. This decay is probably dominated by charge recombination. However, because we cannot exclude the possibility that spin relaxation also contributes to the 5 μs decay time, it represents the lower limit of the radical pair lifetime at 200 K.

Measurements of FcAlPorPh and FcAlPorC₆₀ under the same conditions both give no spin polarized transient EPR signals. This is presumably because of rapid charge separation involving Fc and fast spin relaxation induced by the iron. Thus, the transient EPR data provide only indirect evidence for charge separation in the Fc containing compounds.

Transient Absorption Studies. Nanosecond transient absorption studies provide additional evidence for the formation of charge-separated states and allow their lifetimes to be determined more clearly. We have measured the absorbance difference spectra of the dyads, triad, and their reference compounds in Ar-saturated *o*-DCB solution at ambient temperature. The spectra were collected in the 400–1200 nm range using 532 nm laser light to excite the AlPor moiety. For AlPorPh, the spectrum exhibits the characteristic absorption increase bands at 480 and 820 nm due to formation of the

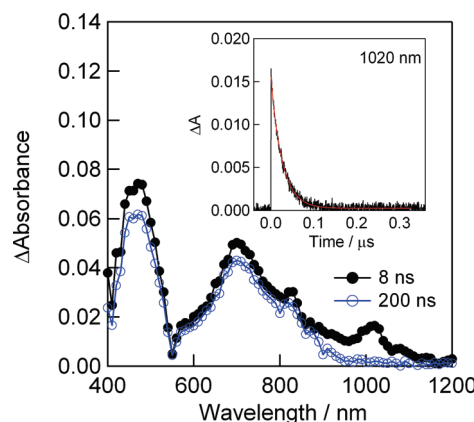


Figure 7. Nanosecond transient absorption spectra of 0.1 mM AlPorC₆₀ induced with 532 nm (ca. 3 mJ/pulse) laser irradiation in Ar-saturated *o*-DCB. Inset: Absorption–time profile.

porphyrin triplet state (Figure S11 in the Supporting Information), and from the decay curve at 480 nm, the lifetime of ³AlPor* was evaluated to be 26 μs . Similarly, the transient absorption spectrum of C₆₀COOMe shows a band at 720 nm corresponding to the fullerene excited triplet state with lifetime of 1.5 μs (Figure S12, Supporting Information).

The transient spectra of the dyad FcAlPorPh (Figure S14, Supporting Information) also show the absorption increase bands of the ³AlPor* moiety at 480 and 820 nm, but the intensity of the absorption increase is smaller and the lifetime is shorter. Additional absorption bands associated with the expected formation of Fc⁺–AlPor[−] are not seen. A possible explanation for the absence of these bands is that charge recombination to the ground state and/or to the lower-lying ferrocene triplet state (³Fc*–AlPor–Ph) may be faster than the instrument response time.

The transient absorption difference spectra of AlPorC₆₀ are shown in Figure 7. The electron transfer from ¹AlPor* to C₆₀ results in the absorption band of the C₆₀[−] moiety at 1020 nm, which decays with a lifetime of 39 ns. The other absorption bands can be assigned to the ³AlPor* state (500 and 820 nm) and the ³C₆₀* state (700 nm), since they decay much more slowly. The expected absorption change due to the AlPor⁺ counterpart of the C₆₀[−] anion is probably buried under the much stronger ³AlPor* and ³C₆₀* absorption bands near 600 nm, since the 39 ns component was not found, except in the 1000 nm region. The time profile at 1020 nm (Figure 7, inset) shows that the absorbance change due to C₆₀[−] rises within the instrument response time, which is consistent with the electron transfer lifetime of ~200 ps that is obtained if the charge separation is assumed to be the dominant fluorescence quenching process. As illustrated in the energy diagram (Figure 3, top right), we estimate a free energy change of $\Delta G = -0.63$ eV for the electron transfer. This value is close in magnitude to the reported reorganization energy for C₆₀ (0.6–0.8 eV),^{69,70} thus, it is likely that the electron transfer is near the top region of the Marcus parabola.⁷¹ However, the transient EPR spectrum of AlPorC₆₀ taken at 80 K (not shown) does not show evidence of radical pair formation in frozen solution, which suggests that either the forward or back electron transfer is not activationless and some solvent reorganization is required.

Since evidence for energy transfer from ¹AlPor* to C₆₀ was observed in the 700–720 nm fluorescence spectra of AlPorC₆₀, it is also possible that the charge separation occurs via ¹C₆₀*. However, the driving force ($\Delta G = -0.24$ eV) for this process is considerably smaller, which probably places it in the normal

region of the Marcus parabola well below the maximum. This would make the electron transfer rate slow and probably observable in the transient absorbance traces. The time profile in Figure 7 does not show any evidence for a component with a slow rise time. Thus, we conclude that intersystem crossing to ${}^3\text{C}_{60}^*$ is the predominant process that occurs from ${}^1\text{C}_{60}^*$. This yields the triplet spectrum seen in the transient EPR data (Figure 6) and the absorption band around 700 nm in the transient absorbance spectrum (Figure 7). From the decay of the absorbance change due to $\text{C}_{60}^{\bullet-}$, the rate constant of the charge recombination and the radical pair lifetime are evaluated as $k_{\text{CR}} = 2.54 \times 10^7 \text{ s}^{-1}$ and $\tau_{\text{RP}} = 39 \text{ ns}$, respectively. This relatively slow charge-recombination rate is caused by the large driving force of 1.51 eV, which leads to $-\Delta G_{\text{CR}} \gg \lambda$ and a high activation energy. The much longer lifetime observed by transient EPR at lower temperature ($\tau_{\text{RP}} \geq 5 \mu\text{s}$ at 200 K) supports the conclusion that the activation energy for the back reaction is large and that it lies in the inverted region of the Marcus parabola.⁷¹ However, care must be taken in inferring the value of the activation energy from the two values of the radical pair lifetime. The radical pair is observable by EPR only in a narrow temperature range around 200 K, which is near the glass transition temperature of the solvent. Thus, the lifetime estimated from the EPR data is not representative of the behavior in liquid solution.

As expected, the electron transfer leads to a much smaller initial absorbance of ${}^3\text{AlPor}^*$ in the dyad AlPorC₆₀ than in the reference compound AlPorPh (0.08 versus 0.30, respectively, at 480 nm). However, this observed reduction by a factor of ~ 4 is smaller than the factor of ~ 10 expected from the fluorescence quenching. It is possible that this difference is due to charge recombination to the triplet states of AlPor and C₆₀. The transient EPR spectrum of the radical pair suggests that the spin–spin coupling is very weak, which leads to very strong singlet–triplet mixing. Under these conditions, triplet recombination becomes the favored pathway because it has a small driving force and the back reaction to the singlet ground state is in the inverted region.

The transient absorbance difference spectra of the triad FcAlPorC₆₀ exhibit many of the same features as those of the dyad AlPorC₆₀ (Figure S13, Supporting Information). An absorption increase band due to $\text{C}_{60}^{\bullet-}$ formation appears at 1020 nm, and bands due to ${}^3\text{AlPor}^*$ (500 and 820 nm) and ${}^3\text{C}_{60}^*$ (700 nm) are also observed. However, a lifetime of 17 ns for $\text{C}_{60}^{\bullet-}$ is obtained from the absorbance difference decay at 1020 nm. This is shorter than the 38 ns obtained for AlPorC₆₀, which is somewhat surprising, since it implies that adding the secondary donor, Fc, does not lead to the expected stabilization of the charge separation due to weaker electronic coupling between the unpaired electrons. A possible explanation for this behavior is that recombination to the Fc triplet state may occur in the triad. The energy of the ${}^3\text{Fc}^*$ (1.16 eV)²⁴ is lower than both charge-separated states $\text{Fc}^+ - \text{AlPor} - \text{C}_{60}^{\bullet-}$ (1.29 eV) and $\text{Fc} - \text{AlPor}^+ - \text{C}_{60}^{\bullet-}$ (1.55 eV) by 0.1–0.4 eV, which should result in a relatively small activation energy for recombination. It is possible that this leads to a faster recombination rate in the triad, despite the expected weaker electronic coupling.

As with the two dyads, the initial absorbance change at 480 ns for the triad is reduced compared to AlPorPh, but the reduction is not as large as predicted from the fluorescence quenching. Again, this difference can be rationalized as the result of either enhanced intersystem crossing and/or triplet recombination of the radical pair states to ${}^3\text{AlPor}^*$.

Photoelectrochemical Studies. To test the photoelectrochemical properties of the dyads and triad, they were deposited onto an OTE/SnO₂ electrode using the electrophoretic deposition method.^{58,59} The absorption spectra of the deposited films of the triad (FcAlPorC₆₀)_n and the dyad OTE/SnO₂/(FcAlPorPh)_n (Figure S15 in the Supporting Information) both exhibit the characteristic porphyrin B-band and Q-band, demonstrating that the complexes were successfully cast on the electrode. However, compared to the solution spectra (Figure 1), they are broadened, indicating significant electronic interaction between neighboring molecules in the film.

TEM images of the cast films (Figure 8) reveal particles that are 50–100 nm in size. Relatively large round particles with diameters of 100–150 nm are visible in the case of (C₆₀COOME)_n (panel A, Figure 8), whereas the dyad (AlPorC₆₀)_n and triad (FcAlPorC₆₀)_n form relatively small interconnected 30–50 nm diameter particles (panels B and D, Figure 8). Further connections are prominent in the image from (FcAlPorPh)_n, and no round particles are seen (panel C, Figure 8). From these observations, the C₆₀ unit appears to be necessary for aggregation into round particles and the AlPor unit is apparently required for the channels connecting the particles to form.

Figure 9 shows the photocurrent action spectra of (AlPorC₆₀)_n, (FcAlPorPh)_n, (FcAlPorC₆₀)_n, and their reference compounds on OTE/SnO₂ electrodes obtained by measuring the photocurrent density as a function of the wavelength of the incident light. The spectra are a plot of the incident photon-to-electron conversion efficiency (IPCE) calculated by normalizing the photocurrent densities for incident light energy and intensity using the following expression:^{58,59}

$$\text{IPCE} (\%) = 100 \times 1240 \times i / (W_{\text{in}} \times \lambda_{\text{ex}}) \quad (1)$$

where i is the photocurrent density (A cm^{-2}), W_{in} is the incident light intensity (W cm^{-2}), and λ_{ex} is the excitation wavelength (in nm). As shown in Figure 9, the IPCE of the OTE/SnO₂/(AlPorC₆₀)_n electrode (panel A, trace a in Figure 9) reaches a maximal value of 24% at 450 nm corresponding to the B-band of the AlPor unit; this IPCE value is 6 times larger than that of OTE/SnO₂/(C₆₀)_n (4% in the 400–450 nm region) and 20 times larger than that of OTE/SnO₂/(AlPorPh)_n (2% at 450 nm). In addition, the IPCE spectrum of the OTE/SnO₂/(AlPorC₆₀)_n electrode has a peak of 20% at 560 nm corresponding to the Q-band of the AlPor unit.

In the case of the Fc-appended dyad (panel B, curve b in Figure 9), the IPCE of the OTE/SnO₂/(FcAlPorPh)_n electrode also has two peaks corresponding to the porphyrin B-band (25% at 450 nm) and Q-band (10% at 560 nm), but they are much narrower than those for the OTE/SnO₂/(AlPorC₆₀)_n electrode. The triad shows similar behavior with peaks of 20% at 450 nm and 15% at 560 nm, which are 5 times larger than those of OTE/SnO₂/(C₆₀)_n. On the basis of these results, we can emphasize the following two points: (i) The combination of the donor and acceptor moieties leads to a large enhancement of IPCE values presumably because of the occurrence of efficient charge separation. (ii) The presence of the C₆₀ unit makes the IPCE spectrum broad. Comparing the spectra of the dyads and triad in Figure 9, it appears that the presence of the C₆₀ moiety leads to the broadening, which is advantageous for solar energy conversion. Thus, the C₆₀-based interpenetrating network among the particles (see Figure 8) appears to play an important role for efficient carrier transport in thin film.

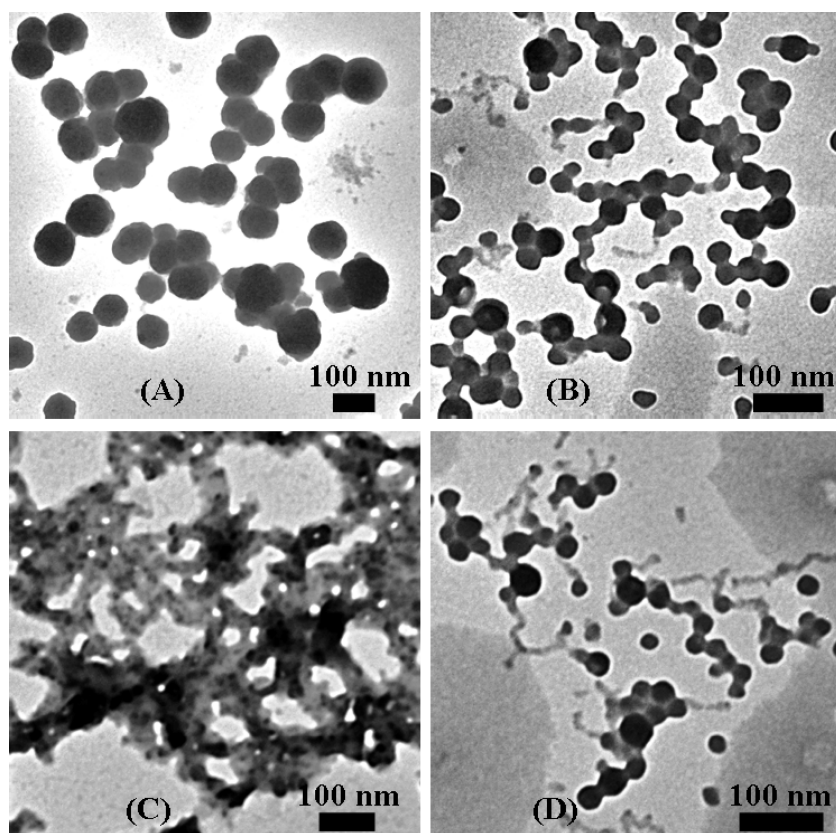


Figure 8. TEM images of (A) $(C_{60}COOMe)_n$, (B) $(AlPorC_{60})_n$, (C) $(FcAlPorPh)_n$, and (D) $(FcAlPorC_{60})_n$.

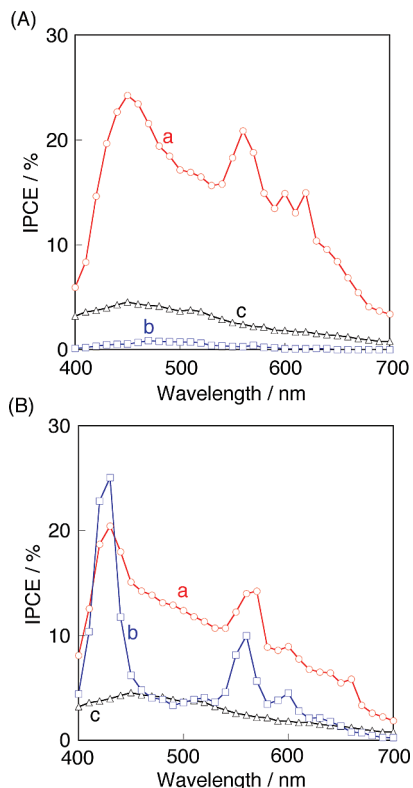


Figure 9. Photocurrent action spectra. (A) (a) OTE/SnO₂/(AlPorC₆₀)_n; (b) OTE/SnO₂/(AlPorPh)_n; (c) OTE/SnO₂/(C₆₀)_n. (B) (a) OTE/SnO₂/(FcAlPorC₆₀)_n; (b) OTE/SnO₂/(FcAlPorPh)_n; (c) OTE/SnO₂/(C₆₀)_n.

Conclusions

Taken together, the spectroscopic data all suggest that light-induced electron transfer takes place in both of the dyads and

the triad. It is significant that the photocurrent action spectrum of the FcAlPorPh dyad clearly shows that excitation of the porphyrin induces charge separation. This is important because although the other methods provide strong indirect evidence for the electron transfer from Fc to AlPor they do not have spectral signatures that can be unambiguously associated with $Fc^{+}-AlPor^{-}$. The results illustrate the utility of AlPor and C₆₀ as building blocks for donor–acceptor systems. The unique structure of C₆₀ results in a small reorganization energy,^{69,70} and it appears that the oxidation midpoint potential of AlPor is such that ΔG for electron transfer to C₆₀ is roughly equal and opposite to the reorganization energy. Thus, the forward electron transfer is essentially activationless. The use of Fc as a secondary electron donor seems to be less advantageous. The lifetime of the charge separated state and the photovoltaic performance on the SnO₂ electrode were not improved by the addition of Fc as expected. We are currently investigating other secondary donors to better understand why this is the case. Finally, the morphology of the nanoparticles deposited on the SnO₂ electrodes apparently plays an important role. The observation of extended structures with channels connecting the nanoparticles is correlated with high photovoltaic performance, which suggests that the channels might provide pathways by which the electron and holes can move on the SnO₂ electrodes.

Acknowledgment. This work was supported by the National Sciences and Engineering Research Council Canada (P.P.K. and A.v.d.E.) and by the PRESTO, Japan Science and Technology Agency (T.H.) and a JSPS fellowship (A.S.D.S.).

Supporting Information Available: Details of spectroscopic experiments, synthesis of the compounds, NMR spectra, absorption spectra, time-resolved fluorescence data, transient absorption

data, and light scattering data. This material is available free of charge via the Internet at <http://pubs.acs.org>.

References and Notes

- (1) Hasobe, T. *Phys. Chem. Chem. Phys.* **2010**, *12*, 44.
- (2) Barber, J. *Chem. Soc. Rev.* **2009**, *38*, 185.
- (3) Gust, D.; Moore, T. A.; Moore, A. L. *Acc. Chem. Res.* **2001**, *34*, 40.
- (4) Sun, L. C.; Hammarstrom, L.; Akermark, B.; Styring, S. *Chem. Soc. Rev.* **2001**, *30*, 36.
- (5) Wasielewski, M. R. *Chem. Rev.* **1992**, *92*, 435.
- (6) Wasielewski, M. R. *J. Org. Chem.* **2006**, *71*, 5051.
- (7) Herrero, C.; Lassalle-Kaiser, B.; Leibl, W.; Rutherford, A. W.; Aukaloo, A. *Coord. Chem. Rev.* **2008**, *252*, 456.
- (8) Scandola, F.; Chiorboli, C.; Prodi, A.; Iengo, E.; Alessio, E. *Coord. Chem. Rev.* **2006**, *250*, 1471.
- (9) Gouterman, M. Optical spectra and electronic structure of porphyrins and related rings. In *The Porphyrins*; Dolphin, D., Ed.; Academic Press: New York, 1978; Vol. 3, p 1.
- (10) Boumaied, I.; Coskun, T.; Stulz, E. Axial coordination to metalloporphyrins leading to multinuclear assemblies. In *Non-Covalent Multi-Porphyrin Assemblies Synthesis and Properties*; Springer: Berlin, 2006; Vol. 121, p 1.
- (11) Maligaspe, E.; Tkachenko, N. V.; Subbaiyan, N. K.; Chitta, R.; Zandler, M. E.; Lemmetyinen, H.; D'Souza, F. *J. Phys. Chem. A* **2009**, *113*, 8478.
- (12) Fukuzumi, S. *Phys. Chem. Chem. Phys.* **2008**, *10*, 2283.
- (13) Albinsson, B.; Martensson, J. *J. Photochem. Photobiol. C* **2008**, *9*, 138.
- (14) Imahori, H.; Hayashi, S.; Hayashi, H.; Oguro, A.; Eu, S.; Umeyama, T.; Matano, Y. *J. Phys. Chem. C* **2009**, *113*, 18406.
- (15) Ohtani, M.; Saito, K.; Fukuzumi, S. *Chem.—Eur. J.* **2009**, *15*, 9160.
- (16) Neugebauer, H.; Loi, M. A.; Winder, C.; Sariciftci, N. S.; Cerullo, G.; Gouloumis, A.; Vazquez, P.; Torres, T. *Sol. Energy Mater. Sol. Cells* **2004**, *83*, 201.
- (17) Xue, J. G.; Uchida, S.; Rand, B. P.; Forrest, S. R. *Appl. Phys. Lett.* **2004**, *85*, 5757.
- (18) Loi, M. A.; Denk, P.; Hoppe, H.; Neugebauer, H.; Meissner, D.; Winder, C.; Brabec, C. J.; Sariciftci, N. S.; Gouloumis, A.; Vazquez, P.; Torres, T. *Synth. Met.* **2003**, *137*, 1491.
- (19) Palomares, E.; Martinez-Diaz, M. V.; Haque, S. A.; Torres, T.; Durrant, J. R. *Chem. Commun.* **2004**, 2112.
- (20) Imahori, H.; Yamada, H.; Guldi, D. M.; Endo, Y.; Shimomura, A.; Kundu, S.; Yamada, K.; Okada, T.; Sakata, Y.; Fukuzumi, S. *Angew. Chem., Int. Ed.* **2002**, *41*, 2344.
- (21) Electron Transfer in Functionalized Fullerenes. In *Fullerenes: From Synthesis to Optoelectronic Properties*; Guldi, D., Martin, N., Eds.; Kluwer Academic Publishers: Norwell, MA, 2002; p 163.
- (22) Martin, N.; Sanchez, L.; Illescas, B.; Perez, I. *Chem. Rev.* **1998**, *98*, 2527.
- (23) Fujitsuka, M.; Ito, O. Photochemistry of Fullerenes. In *Handbook of Photochemistry and Photobiology*; Nalwa, H. S., Ed.; American Scientific Publishers: New York, 2003; Vol. 2 Organic Photochemistry, p 111.
- (24) Araki, Y.; Ito, O. *J. Photochem. Photobiol. C* **2008**, *9*, 93.
- (25) Sandanayaka, A. S. D.; Ito, O. *J. Porphyrins Phthalocyanines* **2009**, *13*, 1017.
- (26) Durr, K.; Fiedler, S.; Linssen, T.; Hirsch, A.; Hanack, M. *Chem. Ber./Recl.* **1997**, *130*, 1375.
- (27) Linssen, T. G.; Durr, K.; Hanack, M.; Hirsch, A. *J. Chem. Soc., Chem. Commun.* **1995**, 103.
- (28) Sastre, A.; Gouloumis, A.; Vazquez, P.; Torres, T.; Doan, V.; Schwartz, B. J.; Wudl, F.; Echegoyen, L.; Rivera, J. *Org. Lett.* **1999**, *1*, 1807.
- (29) Gouloumis, A.; Liu, S. G.; Sastre, A.; Vazquez, P.; Echegoyen, L.; Torres, T. *Chem.—Eur. J.* **2000**, *6*, 3600.
- (30) Guldi, D. M.; Zilberman, I.; Gouloumis, A.; Vazquez, P.; Torres, T. *J. Phys. Chem. B* **2004**, *108*, 18485.
- (31) Guldi, D. M.; Gouloumis, A.; Vazquez, P.; Torres, T. *Chem. Commun.* **2002**, 2056.
- (32) Chen, Y.; El-Khouly, M. E.; Sasaki, M.; Araki, Y.; Ito, O. *Org. Lett.* **2005**, *7*, 1613.
- (33) Kim, K. N.; Choi, C. S.; Kay, K. Y. *Tetrahedron Lett.* **2005**, *46*, 6791.
- (34) Guldi, D. M.; Gouloumis, A.; Vazquez, P.; Torres, T.; Georgakilas, V.; Prato, M. *J. Am. Chem. Soc.* **2005**, *127*, 5811.
- (35) Guldi, D. M.; Ramey, J.; Martinez-Diaz, M. V.; de la Escosura, A.; Torres, T.; Da Ros, T.; Prato, M. *Chem. Commun.* **2002**, 2774.
- (36) Martinez-Diaz, M. V.; Fender, N. S.; Rodriguez-Morgade, M. S.; Gomez-Lopez, M.; Diederich, F.; Echegoyen, L.; Stoddart, J. F.; Torres, T. *J. Mater. Chem.* **2002**, *12*, 2095.
- (37) D'Souza, F.; Ito, O. *Coord. Chem. Rev.* **2005**, *249*, 1410.
- (38) de la Escosura, A.; Martinez-Diaz, M. V.; Guldi, D. M.; Torres, T. *J. Am. Chem. Soc.* **2006**, *128*, 4112.
- (39) Nojiri, T.; Alam, M. M.; Konami, H.; Watanabe, A.; Ito, O. *J. Phys. Chem. A* **1997**, *101*, 7943.
- (40) D'Souza, F.; Gadde, S.; Zandler, M. E.; Itou, M.; Araki, Y.; Ito, O. *Chem. Commun.* **2004**, 2276.
- (41) D'Souza, F.; Smith, P. M.; Zandler, M. E.; McCarty, A. L.; Itou, M.; Araki, Y.; Ito, O. *J. Am. Chem. Soc.* **2004**, *126*, 7898.
- (42) El-Khouly, M. E.; Ito, O.; Smith, P. M.; D'Souza, F. *J. Photochem. Photobiol. C* **2004**, *5*, 79.
- (43) Trabolsi, A.; Elhabiri, M.; Urbani, M.; de la Cruz, J. L. D.; Ajamaa, F.; Solladie, N.; Albrecht-Gary, A. M.; Nierengarten, J. F. *Chem. Commun.* **2005**, *5736*.
- (44) El-Khouly, M. E.; Kang, E. S.; Kay, K. Y.; Choi, C. S.; Aaraki, Y.; Ito, O. *Chem.—Eur. J.* **2007**, *13*, 2854.
- (45) D'Souza, F.; Ito, O. *Chem. Commun.* **2009**, 4913.
- (46) Sandanayaka, A. S. D.; Murakami, T.; Hasobe, T. *J. Phys. Chem. C* **2009**, *113*, 18369.
- (47) Arlt, T.; Schmidt, S.; Kaiser, W.; Lauterwasser, C.; Meyer, M.; Scheer, H.; Zinth, W. *Proc. Natl. Acad. Sci. U.S.A.* **1993**, *90*, 11757.
- (48) Kim, H. J.; Park, K. M.; Ahn, T. K.; Kim, S. K.; Kim, K. S.; Kim, D. H.; Kim, H. J. *Chem. Commun.* **2004**, 2594.
- (49) D'Souza, F.; Maligaspe, E.; Karr, P. A.; Schumacher, A. L.; El-Ojaimi, M.; Gros, C. P.; Barbe, J. M.; Ohkubo, K.; Fukuzumi, S. *Chem.—Eur. J.* **2008**, *14*, 674.
- (50) Fazio, M. A.; Durandin, A.; Tkachenko, N. V.; Niemi, M.; Lemmetyinen, H.; Schuster, D. I. *Chem.—Eur. J.* **2009**, *15*, 7698.
- (51) Davidson, G. J. E.; Tong, L. H.; Raithby, P. R.; Sanders, J. K. M. *Chem. Commun.* **2006**, 3087.
- (52) Kumar, P. P.; Maiya, B. G. *New J. Chem.* **2003**, *27*, 619.
- (53) Metselaar, G. A.; Sanders, J. K. M.; de Mendoza, J. *J. Chem. Soc., Dalton Trans.* **2008**, 588.
- (54) Richeter, S.; Thion, J.; van der Lee, A.; Leclercq, D. *Inorg. Chem.* **2006**, *45*, 10049.
- (55) Podduoori, P. K.; Podduoori, P.; Maiya, B. G.; Prasad, T. K.; Kandashkin, Y. E.; Vasil'ev, S.; Bruce, D.; van der Est, A. *Inorg. Chem.* **2008**, *47*, 7512.
- (56) Aida, T.; Inoue, S. *Acc. Chem. Res.* **1996**, *29*, 39.
- (57) Hirai, Y.; Aida, T.; Inoue, S. *J. Am. Chem. Soc.* **1989**, *111*, 3062.
- (58) Hasobe, T.; Kamat, P. V.; Absalom, M. A.; Kashiwagi, Y.; Sly, J.; Crossley, M. J.; Hosomizu, K.; Imahori, H.; Fukuzumi, S. *J. Phys. Chem. B* **2004**, *108*, 12865.
- (59) Hasobe, T.; Kashiwagi, Y.; Absalom, M. A.; Sly, J.; Hosomizu, K.; Crossley, M. J.; Imahori, H.; Kamat, P. V.; Fukuzumi, S. *Adv. Mater.* **2004**, *16*, 975.
- (60) *Electrochemical Methods: Fundamentals and Applications*, 2nd ed.; Bard, A. J., Faulkner, L. R., Eds.; Wiley: New York, 2001.
- (61) Weller, A. Z. *Phys. Chem.* **1982**, *130*, 129.
- (62) Rehm, D.; Weller, A. *Ber. Bunsen-Ges. Phys. Chem.* **1969**, *73*, 834.
- (63) Harriman, A.; Davila, J. *Tetrahedron* **1989**, *45*, 4737.
- (64) Quimby, D. J.; Longo, F. R. *J. Am. Chem. Soc.* **1975**, *97*, 5111.
- (65) Di Valentin, M.; Bisol, A.; Agostini, G.; Liddell, P. A.; Kodis, G.; Moore, A. L.; Moore, T. A.; Gust, D.; Carbonera, D. *J. Phys. Chem. B* **2005**, *109*, 14401.
- (66) Di Valentin, M.; Bisol, A.; Agostini, G.; Giacometti, G.; Carbonera, D. *Appl. Magn. Reson.* **2006**, *30*, 555.
- (67) Di Valentin, M.; Bisol, A.; Agostini, G.; Carbonera, D. *J. Chem. Inf. Model.* **2005**, *45*, 1580.
- (68) Kobori, Y.; Shibano, Y.; Endo, T.; Tsuji, H.; Murai, H.; Tamao, K. *J. Am. Chem. Soc.* **2009**, *131*, 1624.
- (69) Gadde, S.; Islam, D. M. S.; Wijesinghe, C. A.; Subbaiyan, N. K.; Zandler, M. E.; Araki, Y.; Ito, O.; D'Souza, F. *J. Phys. Chem. C* **2007**, *111*, 12500.
- (70) Imahori, H.; Hagiwara, K.; Akiyama, T.; Aoki, M.; Taniguchi, S.; Okada, T.; Shirakawa, M.; Sakata, Y. *Chem. Phys. Lett.* **1996**, *263*, 545.
- (71) Marcus, R. A. *Angew. Chem., Int. Ed.* **1993**, *32*, 1111.